Applied Catalysis B: Environmental 339 (2023) 123154

Contents lists available at ScienceDirect

Applied Catalysis B: Environmental

journal homepage: www.elsevier.com/locate/apcatb

Tuning the properties of oxygen vacancy around Cu-Mn mixed oxides on dealumination Y zeolite by P-doping to achieve ultra-efficient catalytic ozonation of toluene with low ozone consumption

Qi Shao [a], Zihua Cheng [a], Lei Gao [a], Ting Li [a], Jian Zhang [a,b,*], Chao Long [a,b,*]

[a] State Key Laboratory of Pollution Control and Resource Reuse, School of the Environment, Nanjing University, 163 Xianlin Avenue, Nanjing 210023, China
[b] Quanzhou Institute for Environmental Protection Industry, Nanjing University, Beifeng Road, Quanzhou 362000, China

ARTICLE INFO

Keywords:
P-doping
Dealumination
Cu-Mn oxides
Oxygen vacancy
VOCs

ABSTRACT

As a promising technology, ozone catalytic oxidation can effectively eliminate VOCs at low temperature. However, the excessive ozone consumption brings serious economic problems for industrial applications. Herein, Cu-Mn mixed oxides were supported on the dealumination Y zeolite, and the electronic metal-support interaction between the support and metal nanoparticles was enhanced through P-doping. Satisfyingly, the optimized catalyst P2-CuMn/DY achieved over 90% conversion of toluene even at a very harsh catalytic condition (30 °C, GHSV=240,000 h^{-1}). Moreover, this high toluene conversion accompanying with lower ozone consumption. Compared to CuMn/DY, the ozone/toluene consumption ratio in P2-CuMn/DY decreased from ~ 10:1 to ~ 8.7:1. With the help of multiple various characterizations and DFT calculations, it can be found that the existence of pyrophosphate led more charge to accumulate on the surrounding metal oxides, improving the activity of oxygen vacancies. The change in the properties of oxygen vacancies enhanced the accumulation of O* species on the catalyst, improving the utilization of ozone in the catalytic reaction. This work provides a more economical strategy and guidance to design highly effective catalysts for industrial-scale VOCs eliminations.

1. Introduction

Volatile organic compounds (VOCs), a class of substances with the boiling point below 260 °C under normal pressure and temperature, have become the primary pollutants of atmospheric environmental pollution [1]. In recent years (from 2011 to 2019), the anthropogenic non-methane VOCs emissions in China have increased from 22,976,500 to 27,974,500 tons with an increase of 21.75% [2]. Currently, catalytic combustion technology is one of the most common method to remove VOCs in industrial application because of the its high efficiency and absence of secondary pollution [3]. However, the excessive reaction temperatures not only require more energy consumption, but also have potential security issues. In comparison, ozone catalytic oxidation (OZCO) technology can effectively remove VOCs at low reaction temperatures (below 100 °C), which has been paid an increasing attention by many researchers. Some studies have already reported the excellent VOCs elimination by OZCO at low temperatures or even at the room temperature [4,5]. Unfortunately, the high conversion of VOCs usually requires a high inlet concentration of ozone, which greatly increases the energy consumption and reduces the economic benefit of industrial application [6,7]. Therefore, improving the utilization efficiency of ozone on the premise of ensuring effective degradation of VOCs has become one of the challenges in OZCO technology.

As we all known, ozone can only participate in the degradation of VOCs when it is decomposed and converted into active oxygen species (O*) [8]. The oxygen vacancy in the catalyst has been identified as the effective active site for the decomposition of ozone [9]. At first, some researchers focused on how to increase the amount of oxygen vacancies in the catalyst to achieve better catalytic effect, then, it is gradually recognized that the properties of oxygen vacancy may be the more important factor for turning ozone into O* [10]. Yu et al. once proposed the role of asymmetric oxygen vacancies in oxidation reactions, they thought this type of oxygen vacancy can make the oxygen species become “easy come and easy go” on the surface of the catalyst, facilitating the decomposition of ozone [11]. Recently, Zhang et al. revealed the positive effect of asymmetric oxygen vacancies in Cu-Ce catalysts on

* Corresponding authors at: State Key Laboratory of Pollution Control and Resource Reuse, School of the Environment, Nanjing University, 163 Xianlin Avenue, Nanjing 210023, China.
E-mail addresses: zhj1011@foxmail.com (J. Zhang), clong@nju.edu.cn (C. Long).

https://doi.org/10.1016/j.apcatb.2023.123154
Received 14 February 2023; Received in revised form 1 August 2023; Accepted 4 August 2023
Available online 6 August 2023

VOCs oxidation through static and dynamic quantification tracking [12]. Thus, tuning the properties of oxygen vacancy in the catalyst is an effective method to improve the utilization of ozone, achieving more efficient degradation of VOCs.

Usually, ion doping, etching, reduction and heat treatment are common strategies to improve the properties of oxygen vacancy in the catalyst [10]. Among these methods, the introduction of defects by phosphating has been considered as one of the effective methods [13,14]. P element with rich valence electrons and high electronegativity can affect the structure of oxygen vacancy via the formation of a defective and asymmetrical electronic structure [15]. For example, Huang et al. improved the activity of oxygen vacancy in Pt/CeO_2 by introducing different phosphate structures (POx) [16]. Similarly, Ma et al. enhanced the stability of oxygen vacancy in Bi_2SiO_5 via altering local electronic structure with phosphate dopant [17]. Moreover, the incorporation of POx is more commonly used to promote the electronic metal-support interaction (EMSI) between the catalyst support (such as zeolite) and metal nanoparticles to control the structural properties of the catalysts, which has been widely used in the fields of electrocatalysis, hydrogen evolution, etc. [18,19]. Hendrik et al. proposed in an earlier work that the silicoaluminophosphate (SAPO) interface was formed on the zeolite by phosphate deposition, which can change the micro-load environment of the zeolite support and enhance electron mobility of oxygen species around the loaded metal oxides [20]. Chen et al. also reported the enhancement of EMSI in Pb/Al_2O_3 by tailoring the oxygen mobility and electronic properties with P-doping, achieving more efficient oxidation of methane [14]. Consequently, it is a promising method to improve the properties of oxygen vacancy in the catalyst by P-doping. However, it has not been reported in the field of VOCs degradation by OZCO.

Our previous work reported that Cu-Mn mixed oxides loaded on dealumination Y zeolite (CuMn/DY) can achieve stable and efficient degradation of toluene at low temperatures and high gas velocities, and the specific micro-coordination environment of Al played an important effect on the reaction system [21]. In order to further enhance the catalytic activity of CuMn/DY, the supported P-doped Cu-Mn catalysts containing different phosphate structures were prepared by controlling the concentration of trimethyl phosphate precursor solution in this work. Surprisingly, the toluene conversion of the catalyst was improved once again, moreover, the higher toluene conversion was accompanied by lower ozone consumption. With the help of various characterization techniques, it can be found that the acidity properties and the oxygen vacancy structures were changed in P-doped catalysts. Thus, we discussed in detail about the effects of orthophosphate, pyrophosphate and polyphosphate on the structure and the catalytic performance of the catalysts. In addition, *in situ* DRIFTS technology was used to detect the accumulation process of O* species on the surface of different catalysts and explained the possible reaction mechanism. This study opens up a new theoretical guide to design highly effective catalysts for more economic industrial applications of OZCO technology.

2. Experimental section

2.1. Catalysts preparation

All the materials used in this work were shown in Text. S1. Firstly, the commercial Y zeolite was dealuminated by using steam-nitrate method (650 °C and 0.5 mol/L) that have been reported in our previous research [22]. Then, the impregnation method was used to prepare different catalysts, and the precursor solutions was prepared by dissolving trimethyl phosphate, copper nitrate and manganese nitrate. Specifically, the dealuminated Y zeolite was poured into the prepared precursor solution and the catalysts were obtained by calcination at 550 °C for 4 h in the air after standing at room temperature for 12 h and drying at 110 °C for 12 h. Finally, the different catalysts were named as CuMn/DY (P:Cu:Mn=0:1:1), P2-Mn/DY (P:Cu:Mn=2:0:1), P2-Cu/DY (P:Cu:Mn=2:1:0), P1-CuMn/DY (P:Cu:Mn=1:1:1), P2-CuMn/DY (P:Cu:Mn=2:1:1) and P3-CuMn/DY (P:Cu:Mn=3:1:1) according to different molar ratio of P, Cu and Mn.

2.2. Catalysts characterization

The catalysts were characterized by Brunauer−Emmett−Teller (BET) method, Inductively coupled plasma optical emission spectrometry (ICP-OES), Fourier transform infrared (FT-IR) spectroscopy, Ultraviolet–visible (UV–vis) spectroscopy, X-ray diffraction (XRD), Scanning electron microscope (SEM), High Resolution Transmission Electron Microscope (HRTEM), ^{31}P magic angle spinning nuclear magnetic resonance (^{31}P MAS NMR), Electron paramagnetic resonance (EPR), Raman spectra (Raman), temperature-programmed desorption of ammonia (NH_3-TPD), temperature-programmed desorption of oxygen (O_2-TPD), H_2 temperature-programmed reduction (H_2-TPR), X-ray photoelectron spectroscopy (XPS) and *in situ* diffuse reflectance infrared fourier transform (*in situ* DRIFTS). The detailed characterization methods are described in Text. S1.

2.3. DFT calculations

The detailed modeling and calculation method of density functional theory calculation are shown in Text. S1.

2.4. Catalytic performance evaluation

The catalytic performance of different catalysts was evaluated by using the experimental device in Fig. S1. The detailed experimental conditions and calculation formulae are shown in Text. S1.

3. Results and discussion

3.1. Catalytic performance

The toluene conversion on different catalysts was shown in Fig. 1a. It can be seen that the degradation performance of toluene increased first and then decreased with increasing the amount of P incorporation. P2-CuMn/DY exhibited the best catalytic performance with nearly 90% toluene conversion even at a very harsh catalytic condition (30 °C, GHSV=240,000 h^{-1}). However, the higher phosphorus content (P3-CuMn/DY) had a negative effect on the catalytic reaction. Although P2-Cu/DY and P2-Mn/DY contained the same phosphorus content as P2-CuMn/DY, the former without Mn rapidly deactivated and the toluene conversion dropped to about 8% after 120 min (Fig. S2), and the latter without Cu exhibited worse catalytic performance than CuMn/DY. The above results indicated that MnOx is the active site for the catalytic reaction, while the Cu and P component only acted as the co-catalyst. Accordingly, the turnover frequency (TOF_{Mn}) of different catalysts were estimated and the value of P2-CuMn/DY was significantly higher than that of other catalysts (Fig. S3). In addition, interestingly, the ratio of decomposition rate of ozone to toluene decreased significantly for the catalysts after P-doping and did not change with the phosphorus content (Fig. 1c), it implies that the introduction of phosphorus can optimize the path of toluene oxidation, and improve the ozone utilization of the catalysts. Satisfyingly, all of the catalysts exhibited over 90% conversion of toluene after appropriately reducing the gaseous hourly space velocity (GHSV=170000 h^{-1}) of the catalytic reaction and P-doped catalysts still maintained a low consumption ratio of ozone/toluene (Figs. S4 and S5). Compared with the CuMn/DY, the selectivity of CO_2 in the P-doped catalysts was slightly improved (Fig. S6).

The stability and moisture resistance of the catalysts are of great significance for industrial exhaust emissions. It can be seen from Fig. 1d that the optimized catalyst P2-CuMn/DY can still maintain a stable toluene conversion even in a long reaction time, accompanying by a slow decline in ozone decomposition. The humidity cycling experiments

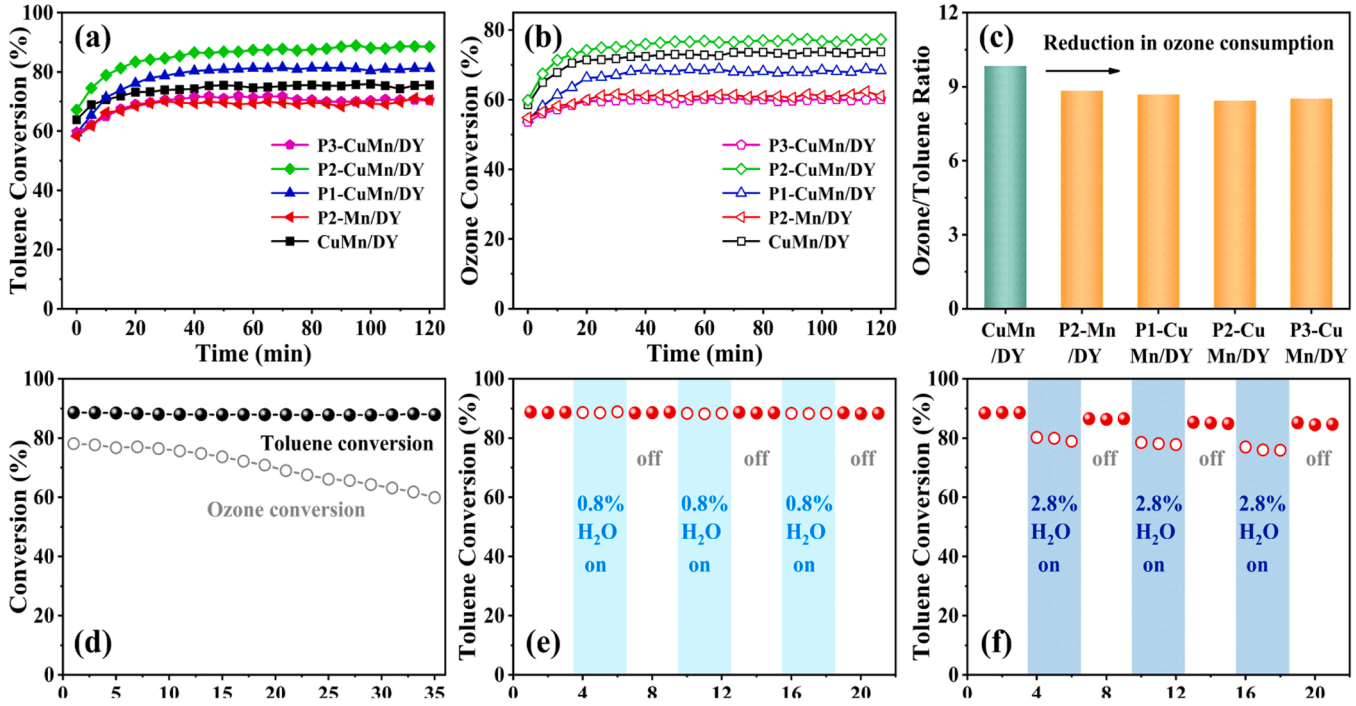

Fig. 1. (a) Conversion of toluene, (b) conversion of ozone and (c) ozone/toluene decomposition ratio of different catalysts; (d) stability test of P2-CuMn/DY; (e) low humidity and (f) high humidity cycling test of P2-CuMn/DY. [ozone] = 2000 ppm, [toluene] = 200 ppm, 30 °C, GHSV= 240,000 h^{-1}.

show that low content of water vapor (0.8%) has no effect on the catalytic performance of P2-CuMn/DY (Fig. 1e). When a high content of water vapor (2.8%) was introduced into the reaction system, the toluene conversion of P2-CuMn/DY decreased by about 10% (Fig. 1f). However, it can be recovered quickly after water off, and the toluene conversion was almost the same as that before water injection. It can be concluded that only very few active sites in the catalyst were irreversibly inactivated, the majority of the catalytic sites can be recovered by switching to dry gas flow. The toluene conversion of P2-CuMn/DY decreased only about 5% after three cycles, which indicates that the catalyst has excellent moisture resistance. In addition, the catalytic activity of the catalyst can be quickly restored by a simple heating (Fig. S7).

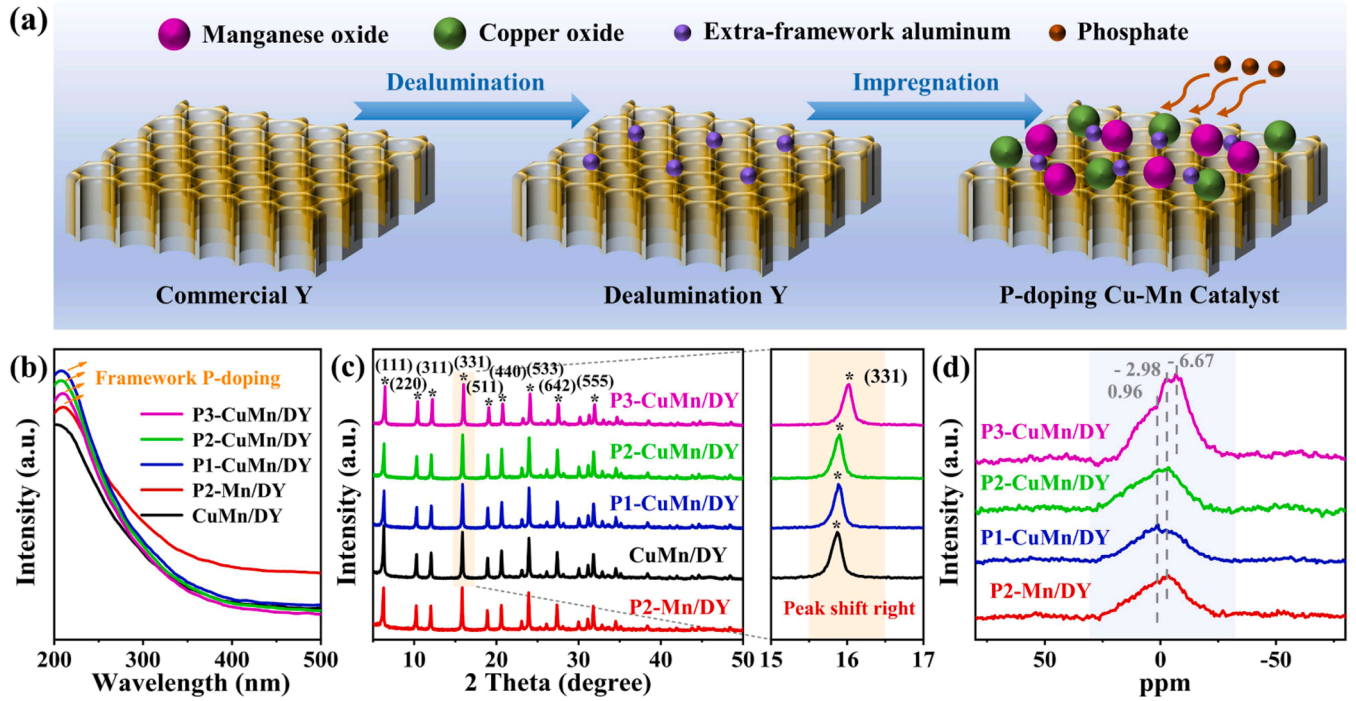

Fig. 2. (a) The preparation diagram of the catalysts; (b) DR UV–vis spectra, (c) XRD patterns and (d) ^{31}P MAS NMR spectra of different catalysts.

3.2. Characterization of catalysts

3.2.1. Structural and crystal properties

Fig. 2a shows the preparation diagram of the catalysts. The results of ICP-OES show that the contents of P, Cu and Mn in the catalysts are consistent with the theoretical loading (Table S1). Fig. S8 shows the N_2 adsorption-desorption isotherms and the pore structure parameters of all the catalysts are shown in Table S1. It is known that the variation of specific surface area and pore volume was less than 10% for several catalysts after P-doping, indicating that the phosphates did not destroy the pore structure of the zeolite support. This slight change in specific surface area and pore volume may not have great effect on the catalytic reaction.

It is noticeable that the introduction of phosphate had a very important effect on the structure of the catalysts. POx, which was doped in the catalyst, is usually associated with the stretching vibration peaks at around 677 and 927 cm^{-1} in FT-IR spectra [17]. Unfortunately, because of the low content of phosphorus in the catalysts, these weak response signals were covered by the strong absorption peaks of the zeolite framework vibration [23], which makes it difficult to distinguish the P-O structure in different catalysts from FT-IR spectra (Fig. S9). However, a new signal can be observed at around 208 nm in DR UV–vis spectra for P-doped catalysts (Fig. 2b). This absorption band is suggested to be related to the charge transfer transitions between framework heteroatom species and lattice O^{2-} in the zeolite [24], which means that P species were successfully incorporated into the framework of the zeolite. Coincidentally, another strong proof comes from XRD patterns. As shown in Fig. 2c, the typical Y zeolite characteristic peak can be observed in all of the catalysts [25], which shows that the process of dealumination did not damage the main structure of the zeolite support. However, interestingly, the characteristic peak of the catalysts shifted to the right with the increase of P incorporation, which is because that P-O band is shorter than Si-O and Al-O band in the zeolite, leading to the lattice shrinkage [26,27]. It is consistent with the results of DR UV–vis, indicating that POx had been successfully introduced into the framework of the zeolite. The characteristic peak of P3-CuMn/DY shifted to the right more significantly compared with other catalysts, which indicates that the different phosphorus content can lead to different structure of POx in the catalyst. When the phosphorus content increased to a certain amount, more P species can be inserted into the lattice of the catalyst. However, the characteristic peaks of POx, CuOx and MnOx cannot be detected from the XRD patterns, it is due to the fact that the low content of these components are highly dispersed on the support, which can be proven by the results of SEM-EDS (Fig. S10).

Additionally, the microstructure of CuOx and MnOx can be observed in HRTEM images. As shown in Fig. S11, the metal nanoparticles were successfully loaded on the zeolite support, and the different lattice fringes of copper oxides and manganese oxides can be observed, including 0.199 nm, 0.248 nm, 0.346 nm and 0.489 nm belonged to MnO_2 (130), Mn_3O_4 (211), MnO_2 (220) and MnO_2 (200) [5,21], 0.232 nm and 0.253 nm belonged to CuO (111) and CuO (002), respectively [12,21].

The ^{31}P MAS NMR can be used to further determine the subtle differences of P species in different catalysts. As shown in Fig. 2d, a strong peak at around 0.96 ppm and a broad peak at around - 2.98 ppm were detected in P1-CuMn/DY, which can be associated to the characteristic signal of isolated orthophosphate and pyrophosphate, respectively [28]. For P2-Mn/DY and P2-CuMn/DY, the proportion of pyrophosphate increased obviously, which implicated that orthophosphate was formed first in the catalyst with low phosphorus content and more pyrophosphate can be generated by the orthophosphate self-assembly as the phosphorus content of the catalyst increased. Comparatively, the P3-CuMn/DY catalyst with higher phosphorus content showed a new peak at around - 6.67 ppm, which can be attributed to polyphosphates [29]. Combined with the results of XRD (Fig. 2c), the polyphosphates can be more easily inserted into the lattice of P3-CuMn/DY, it probably because that the OH bond around the polyphosphate is more easily to break down and combine with the zeolite support after calcination [20]. These different structures of POx may have an important effect on the catalytic performance of the catalysts.

3.2.2. Acidic properties

We have reported in detail about the relationship between acidic properties of Y-zeolite catalysts and catalytic oxidation of toluene in a previous work [30]. It has been found that the acid sites, especially Lewis acid, can promote the adsorption and activation process of toluene, improving the efficiency of toluene ozonation. Therefore, the acidity of different catalysts was evaluated. NH_3-TPD can roughly reflect the acidity change of the catalysts. Usually, the adsorption peak at around 120 °C can be correspond to the weak acid sites while the adsorption peak above 350 °C represents strong acid sites in the materials [31]. Besides these two peak signals, a new shoulder peak appears at 200–300 °C in Cu-containing catalysts, which cannot be observed in the single Mn catalyst (Fig. S12a). It has been confirmed to be related to the new medium strong acidic sites formed by strong Cu-Mn interactions on the support [32], and this peak signal is similar in CuMn/DY and P-doped catalysts, which implies that the existence of POx does not destroy this acidic structure. To further accurately quantify the acidic sites in the catalysts, pyridine-adsorbed FT-IR spectra of different catalysts were determined at 303, 473 and 623 K, and the calculation results are shown in Table S2. As shown in Fig. S12b-f, the absorption bands at around 1450, 1490 and 1620 cm^{-1} correspond to Lewis acid sites while the absorption bands at around 1490, 1545 and 1635 cm^{-1} represent Brønsted acid sites in the catalyst [33,34]. In addition, the absorption bands at around 1575 and 1600 cm^{-1} were also observed, which can be attributed to the physical adsorption of pyridine molecules [35]. The peak intensities at different test temperatures reflect the binding strength between pyridine and the acid sites, which can represent the acidity strength on the surface of the catalysts. As shown in Table S2, the amount of Brønsted acid sites in three P-doped catalysts (P1-CuMn/DY, P2-CuMn/DY and P3-CuMn/DY) increased compared with CuMn/DY, which may be related to the hydroxyl group attached to the end of POx (P-OH) [20]. The amount of Brønsted acid sites in single Mn catalyst (P2-Mn/DY) was more than that in Cu-Mn catalysts, which indicates that some of P-OH defects bind to Cu-Mn nanoparticles to eliminate part of Brønsted acid sites. In addition, the amount of Lewis acid sites in Cu-Mn catalysts increased significantly compared with P2-Mn/DY, which suggests that the newly formed acidic sites detected in NH_3-TPD may be associated with Lewis acid sites. Combining the results of toluene conversion and the pyridine FT-IR, it is known that the toluene conversion on several catalysts followed the same order as Lewis acid concentration: P2-Mn/DY < CuMn/DY < P1-CuMn/DY < P2-CuMn/DY, and a strong linear relationship can be observed between the toluene conversion and the amount of Lewis acid sites (Fig. 3). However, the Brønsted acid sites in the catalysts have poor correlation with the degradation of toluene (Fig. 3). The above results suggest that the different structures of POx can act in synergy with the metal nanoparticles to change the acidity of the catalysts, consequently affecting the oxidation efficiency of toluene. Specially, the data of P3-CuMn/DY is not included in the linear fitting in Fig. 3, it is because that the catalytic performance of P3-CuMn/DY is worse than that of CuMn/DY without P-doping even though it contains more Lewis acid sites, suggesting that there are other factors playing a crucial role in catalytic ozonation system, which will be discussed in the following section.

3.2.3. Oxygen vacancies and chemical structural properties

It is well-known from Fig. 1c that P-doping decreased significantly the consumption ratio of ozone/toluene of the catalysts, which means that P-doping enhanced the ability of the catalysts to decompose ozone into active oxygen species (O*). A lot of evidences have showed that the oxygen vacancies in the catalyst are the active sites for decomposition of ozone [12,36]. Therefore, the properties of oxygen vacancies and the

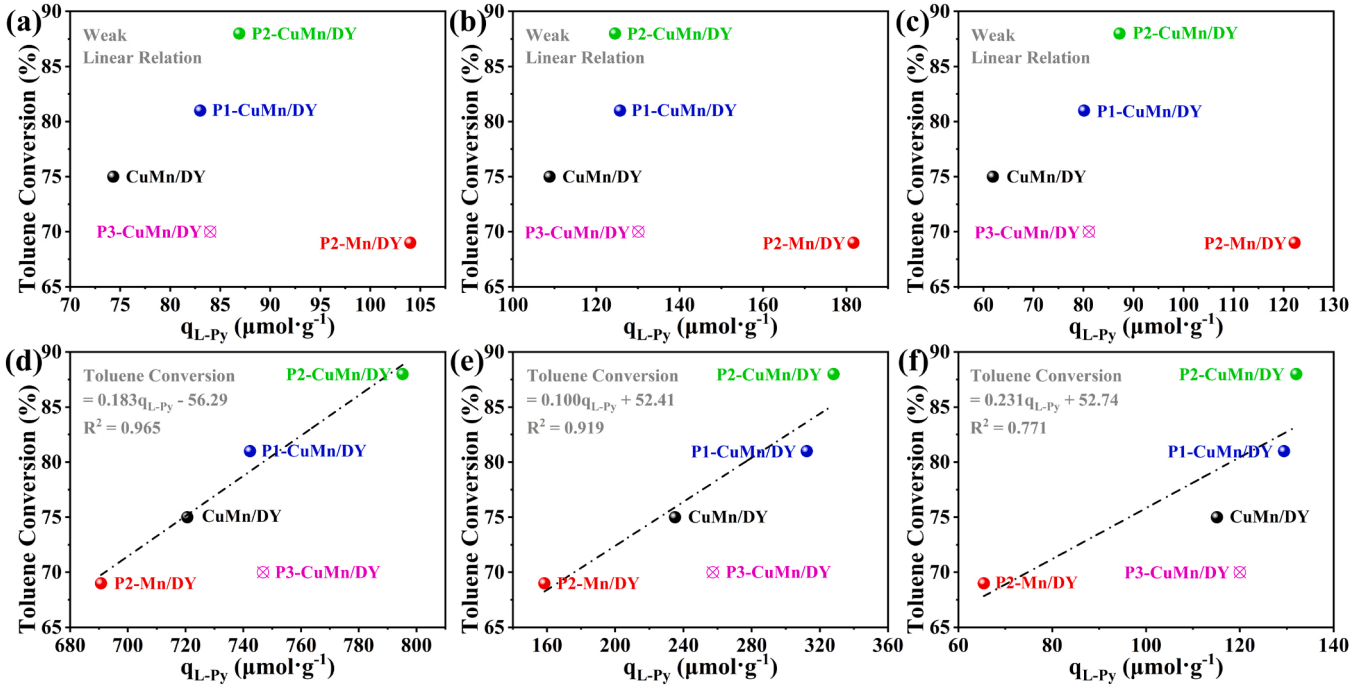

Fig. 3. The relationship between Brønsted / Lewis acid sites and toluene conversion of different catalysts: (a) Brønsted acid sites at 303 K, (b) Brønsted acid sites at 473 K, (c) Brønsted acid sites at 623 K, (d) Lewis acid sites at 303 K, (e) Lewis acid sites at 473 K and (f) Lewis acid sites at 623 K.

ability of ozone decomposition in different catalysts were evaluated comprehensively. EPR is considered to be a common technique for identifying oxygen vacancies in nanomaterials, the presence of oxygen vacancies is revealed by the signal of unpaired electrons at around g= 2.003 [37]. As shown in Fig. 4a, the signal at g= 2.003 representing oxygen vacancy was detected in all of the catalysts. Different from the other four catalysts, the signal strength in P3-CuMn/DY decreased significantly, which indicates a decrease in the amount of oxygen vacancies, corresponding with the poorer catalytic performance of P3-CuMn/DY even if it had higher amount of Lewis acid sites. Interestingly, a new EPR signal at g= 1.998 was only observed in P2-CuMn/DY, which can be attributed to structural disturbance by POx on the surface of the catalyst. This newly formed unsaturated coordination electron structure may promote the electron transfer around oxygen vacancies, improving the ozone decomposition ability of the catalyst, which corresponds to the best catalytic performance of P2-CuMn/DY. Even though P2-Mn/DY contained the similar amount of pyrophosphate to P2-CuMn/DY, this electron-deficient structure was also not detected, indicating that pyrophosphate can only interacted with the Cu-Mn mixed oxides to produce this “defect”.

O_2-TPD can be used to further investigate the different properties of oxygen species in the catalysts. As shown in Fig. 4b, the peak signal below 300 °C belongs to adsorbed oxygen species (O_{ads}), 300–600 °C peak signal belongs to lattice oxygen species (O_{latts}), and the response signal at higher temperature (over 600 °C) belongs to bulk phase lattice oxygen species ($O_{b\text{-}latts}$) in the interior of the materials, respectively [37]. A strong desorption peak representing O_{latts} can be observed in P3-CuMn/DY, which cannot be detected in other catalysts. It means that the oxygen species around polyphosphate formed in P3-CuMn/DY were embedded into the lattice of the material leading to an increase in the ratio of lattice oxygen species in the catalyst, which is consistent with the results of XRD and ^{31}P MAS NMR (Fig. 2c and d) However, the lattice oxygen species only activated at high temperature are difficult to participate in the low temperature OZCO reaction. The higher ratio of lattice oxygen species in P3-CuMn/DY leads to a decrease in the amount of oxygen vacancies, which is highly consistent with the results of EPR (Fig. 4a). Therefore, the poor catalytic performance of P3-CuMn/DY may be related to the weak ability of ozone decomposition. In addition, the desorption temperatures of O_{ads} in P-doped catalysts were significantly lower than that of CuMn/DY. It indicates that the introduction of POx can enhance the mobility of adsorbed oxygen species, leading the surrounding oxygen vacancies more active to improve the ability of ozone decomposition. Although the EPR signal of g= 1.998 was not detected in P2-Mn/DY (Fig. 4a), the desorption temperature of O_{ads} was still lower than that in P1-CuMn/DY and P3-CuMn/DY, which implies that pyrophosphate can enhance the activity of oxygen vacancies in catalyst. Compared to P2-Mn/DY, P2-CuMn/DY showed the lower desorption temperature of O_{ads}, which means that the unsaturated coordination electron structure detected in EPR can further change the coordination state of O around Cu-Mn mixed oxide to affect the properties of the surrounding oxygen vacancies.

Raman spectra was used to further evaluate the O coordination state for better understanding the properties of oxygen vacancies of the catalysts. As shown in Fig. 4c, a strong signal at 460 cm^{-1} can be observed in P2-Mn/DY, which has been confirmed to be related to the vibration of Y zeolite framework [38]. This peak signal shifted blue to 505 cm^{-1} in Cu-Mn catalysts, indicating that the introduction of Cu enhanced the interaction between the zeolite support and metal nanoparticles. The weak signal between 570 and 650 cm^{-1} can be attributed to the vibration of the Mn-O bond [39]. It can be still observed that the blue shift of Mn-O in Cu-Mn catalyst after P-doping although the peak signal is not obvious due to the low content and high dispersion of MnOx, which means that the binding force of Mn-O bond becomes looser, and the oxygen vacancies around MnOx become more active. Two typical peaks of CuO can be detected at 296 and 346 cm^{-1}, corresponding to A_g and B_g modes of CuO [40]. As the same with Mn-O bond, the blue shift of Cu-O bonds can be also observed in P-doped catalysts, which further indicates that POx can change the coordination environment of O around metal nanoparticles. Additionally, the signal between 765 and 905 cm^{-1} can be detected in P1-CuMn/DY, P2-CuMn/DY and P3-CuMn/DY. It may be due to structural vibrations caused by the introduction of P, which cannot be observed in CuMn/DY and P2-Mn/DY. It also implies that there may be a strong interaction between POx and Cu-Mn mixed oxide, which may change the structure of the coordination O in the catalyst and

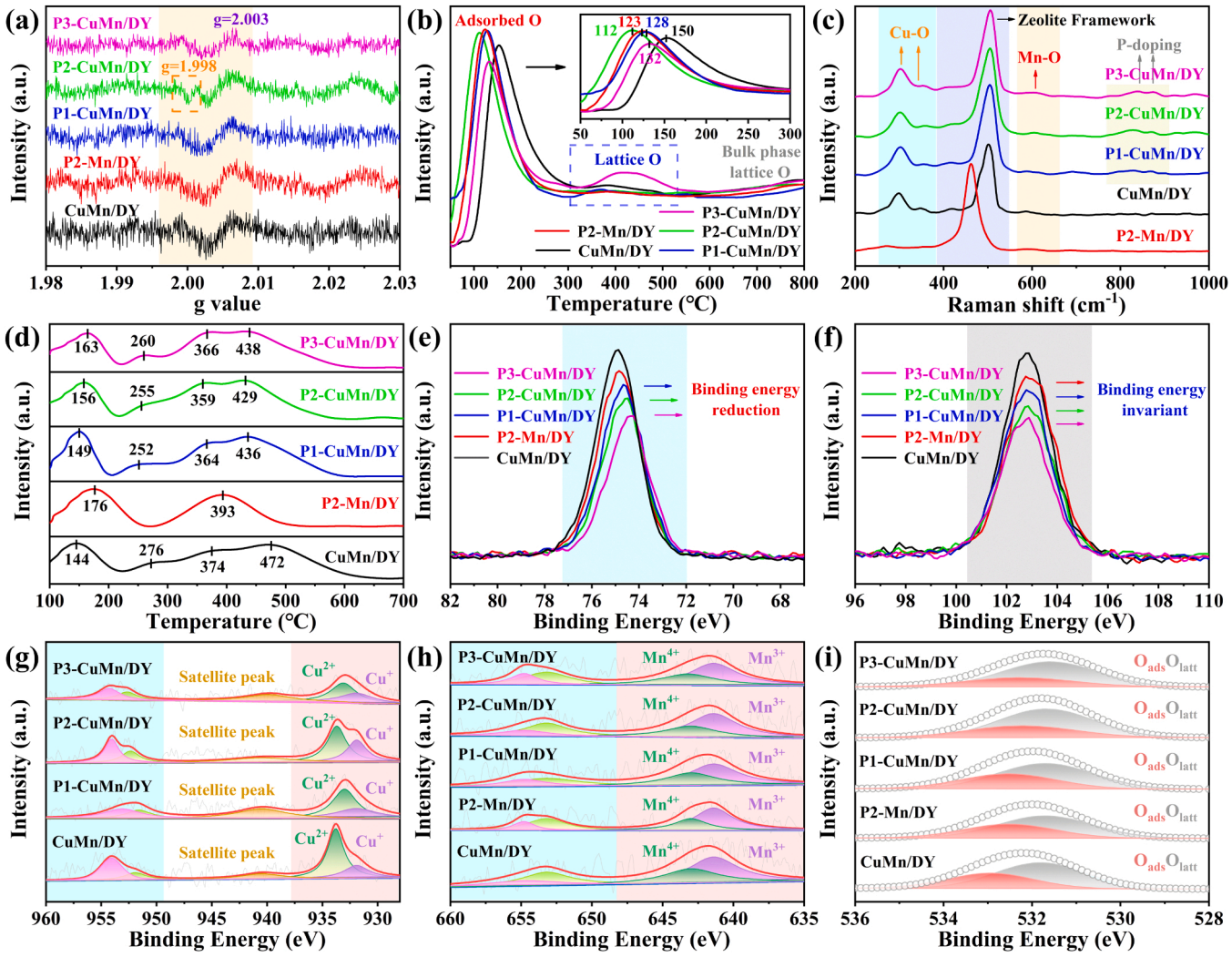

Fig. 4. (a) EPR profiles, (b) O_2-TPD profiles, (c) Raman spectra, (d) H_2-TPR profiles and (e) Al 2p, (f) Si 2p, (g) Cu 2p, (h) Mn 2p, (i) O 1 s XPS spectra of different catalysts.

affect the properties of the surrounding oxygen vacancies. It is consistent with the results of EPR and O_2-TPD.

The chemical properties of metal oxides in the catalysts were characterized by using H_2-TPR (Fig. 4d). Two signal peaks below 500 °C were observed in P2-Mn/DY, which can be attributed to the two reduce processes of $MnO_2 \rightarrow Mn_2O_3$ (low temperature) and $Mn_2O_3 \rightarrow Mn_3O_4$ (high temperature), respectively [41]. Compared to the single Mn catalyst, the reduction peak position of Mn in CuMn/DY with and without P-doping moved to low temperature, indicating that the introduction of Cu enhanced the reduction ability of the catalyst. Besides, the peak signal around 472 °C in CuMn/DY can be associated with the reduce processes of CuOx [42]. With the increased of P content, the position of the first reduction peak in P-doped catalysts moved slightly to high temperature, which means that the introduction of POx can lead to a slight decrease in the reducibility of the catalyst. However, the peak signal between 200 and 300 °C, which is related to the strong interfacial effect formed by electron transfer between Cu-Mn mixed oxides [21], moved to low temperature in P-doped catalysts, and the signal area increased significantly in P2-CuMn/DY, which is consistent with the previous discussion that POx can interact with active metal component and pyrophosphate may have stronger electron transfer effect with Cu-Mn mixed oxides. Moreover, the CuOx and MnOx reduction peaks at 300–500 °C moved to low temperature in P-doped catalysts, which also confirmed the existence of the strong interaction between POx and metal nanoparticles. This strong electron transfer can make the oxygen species around the loading metal oxides to become more active, increasing the ozone decomposition ability of surrounding oxygen vacancies, which is conducive to the conversion of toluene. Therefore, P2-CuMn/DY with the strongest signal of the Cu-Mn interaction showed the best catalytic performance.

In order to evaluate the surface chemical properties and further investigate the influence of the interaction between POx and metal nanoparticles on the oxygen vacancies of the catalysts, XPS was used to detect the microelectronic coordination environment of different elements. The XPS spectra of P 2p was shown in Fig. S13. Unfortunately, the weak P signal peak can be only detected in P3-CuMn/DY due to the low content of P in the other catalysts. However, the effect of P on oxygen vacancies can be revealed through the electronic structure change of other elements. As shown in the XPS spectra of Al 2p and Si 2p (Fig. 4e and f), the peak signal of the catalysts with higher P content became weaker, indicating that some POx covered on the surface of the zeolite support, the slight drop in the peak signal of P2-Mn/DY may be due to less metal content in the catalyst. Interestingly, with the increase of P content in the catalysts, the binding energy of Al decreased and the density of surrounding electron cloud increased, which cannot be observed in the element of Si. It shows that POx can coordinate with Al rather than Si in the zeolite support to form Al-O-P bond, which is consistent with the conclusion reported by Hendrik et al. that Si-O-P

bond is unstable in the zeolite [20]. This new formed Al-O-P bond may be the key of the strong interaction between the zeolite support and the metal oxides. However, compared with CuMn/DY, the binding energy of Al in P2-Mn/DY was not decreased, which suggests that the influence of Cu on the supported environment of the catalyst cannot be ignored. Furthermore, the effect of strong electronic metal-support interaction on the oxygen vacancies in catalysts can be also revealed in the Cu 2p and Mn 2p XPS spectra. As shown in Fig. 4g and h, the convolution peaks of Cu^{+} (~ 932.5 eV), Cu^{2+} (~ 934.2 eV), Mn^{3+} (~ 641.4 eV) and Mn^{4+} (~ 643 eV) can be divided according to different binding energy in Cu $2p_{3/2}$ and Mn $2p_{3/2}$, respectively [43,44]. Compared with CuMn/DY, the binding energy of Cu and Mn decreased in three P-doped catalysts, which indicates that the introduction of P leads to the increase of electron cloud density around the metal oxides, which is beneficial to promote the electron transfer between the surrounding coordination O to improve the activity of the oxygen vacancies. As shown in Table S3, the Cu^{+}/Cu^{2+} and Mn^{3+}/Mn^{4+} ratio firstly increased and then decreased with the increase of P content in the catalysts, which means that POx promotes the formation of low valent metal oxides, and the interaction between pyrophosphate and metal oxides is more significant. Specially, the binding energy of Mn did not decrease obviously in P2-Mn/DY (Fig. 4h), which is consistent with the previous discussion that the electron transfer between POx and single Mn is not as strong as that between POx and Cu-Mn mixed oxides. Even so, the Mn^{3+}/Mn^{4+} ratio of P2-Mn/DY is higher than that of CuMn/DY, the lower valent Mn^{3+} has been thought to be related to oxygen vacancies in MnOx [45], which means that the oxygen vacancies around MnOx in P2-Mn/DY may have a stronger electron mobility than CuMn/DY. Fig. 4i shows the XPS spectra of O 1 s, two asymmetric peaks can be divided at around 532.1 and 533.2 eV, which belong to lattice oxygen (O_{latts}) and adsorbed oxygen (O_{ads}), respectively [46]. It can be seen that the O_{ads}/O_{latts} ratio decreased with the increased of P content in the catalysts (Table S3), the content of O_{ads} in P3-CuMn/DY was the lowest, which can be related to the amount of oxygen vacancies in the catalysts. It is consistent with results of EPR (Fig. 4a) that excess phosphate leads to a decrease in the amount of oxygen vacancies. In short, as shown in Fig. 5, the phosphates supported on the zeolite can promote the electronic metal-support interaction to affect the properties of oxygen vacancies in the catalyst. Specially, a stronger EMSI existed between pyrophosphate and Cu-Mn mixed oxides, which leads the surrounding oxygen vacancies to become more active, corresponding to the best catalytic performance of P2-CuMn/DY.

The DFT calculations further confirmed the effect of pyrophosphate on electron transfer at Cu-Mn interface. According to the results of HRTEM (Fig. S11), the theoretical models of MnO_2 (200), pyrophosphate-MnO_2 (200), CuO (002)/MnO_2 (200), pyrophosphate-CuO (002)/MnO_2 (200) were established (Figs. S14 and S15). It can be seen from Fig. 6 that the charge accumulation occurred around pyrophosphate, which causes the O in the metal oxide near pyrophosphate to become more active, enhancing the activity of the surrounding oxygen vacancies. The existence of CuO led more charge to be transferred to the vicinity of pyrophosphate (Table S4), making the properties of oxygen vacancies at Cu-Mn interface more active. Although the charge accumulation around the manganese atom decreases, the Bader charge calculations (Tables S5 and S6) show that the electronegativity of MnO_2 increases in pyrophosphate-CuO (002)/MnO_2 (200) compared to pyrophosphate-MnO_2 (200), which means that more negative charge accumulates in the coordinated O atoms, increasing the activity and mobility of oxygen species. Therefore, ozone may be more easily decomposed and converted into active oxygen species (O*) on the surface of Cu-Mn catalyst containing pyrophosphate.

3.3. *In situ* DRIFTS of ozone adsorption

In situ DRIFTS of ozone adsorption can reflect the differences in the adsorption and decomposition of ozone on the surface of different catalysts. As shown in Figs. 7a-7e, the peak signals at ~ 835 cm^{-1}, ~ 1015 cm^{-1}, ~ 1165 cm^{-1} and ~ 1205 cm^{-1} can be observed in all of the catalysts. The weak band at ~ 835 cm^{-1} belongs to O_3^-, which is considered to be an intermediate in the process of ozone decomposition [47,48]. The band at ~ 1015 cm^{-1} can be attributed to the physical adsorption peak of ozone molecules on the surface of the catalysts [47, 48]. In addition, the bands at ~ 1165 cm^{-1} and ~ 1305 cm^{-1} can be ascribed to O_2^- ion and atomic oxygen O^- species, which are usually considered to be the active oxygen species (O*) with oxidizing property [47,48]. The signal peak of O^- species in P-doped catalysts was slightly blue shifted, which may be due to the fact that the introduction of POx changed the property of the oxygen vacancy in the catalyst, resulting in the weaker binding ability of the generated O^- species to the catalyst surface. Thus, the active oxygen species can migrate more rapidly to oxidize adsorbed substances. Additionally, the accumulation of O^- species of the five catalysts was significantly different in the same time range (Fig. 7f). P2-CuMn/DY has the highest accumulation of O^- species, corresponding to the most active oxygen vacancies and the best catalytic performance of the catalyst. Although the accumulation of O^- species in P2-Mn/DY was also relatively high, the poor acidity of the catalyst led to a bad catalytic performance. Similarly, another active oxygen species O_2^- showed the same accumulation trend to O^- species in all of the catalysts (Fig. S16). Different from the other catalysts, the response signals of all intermediates are weaker in P3-CuMn/DY, it is because although the oxygen vacancies in P3-CuMn/DY are relatively active, the amount of oxygen vacancies is too small to cause some of ozone cannot be decomposed into O* to participate in the oxidation of toluene. In contrast, even though the amount of oxygen vacancies in P2-CuMn/DY is not the highest, the properties of oxygen vacancies are the most active among all catalysts, corresponding to the best conversion of toluene. It suggests that the activity of the oxygen vacancies was the key factor to determining the catalytic oxidation reaction when the amount of oxygen

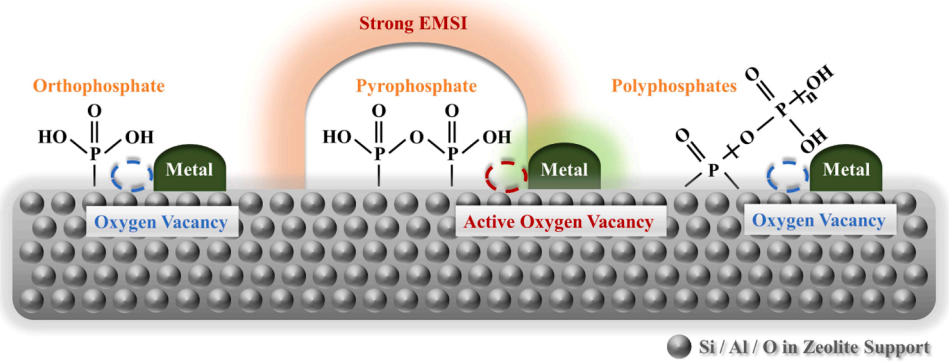

Fig. 5. The effect of different phosphates on the oxygen vacancy in the catalysts.

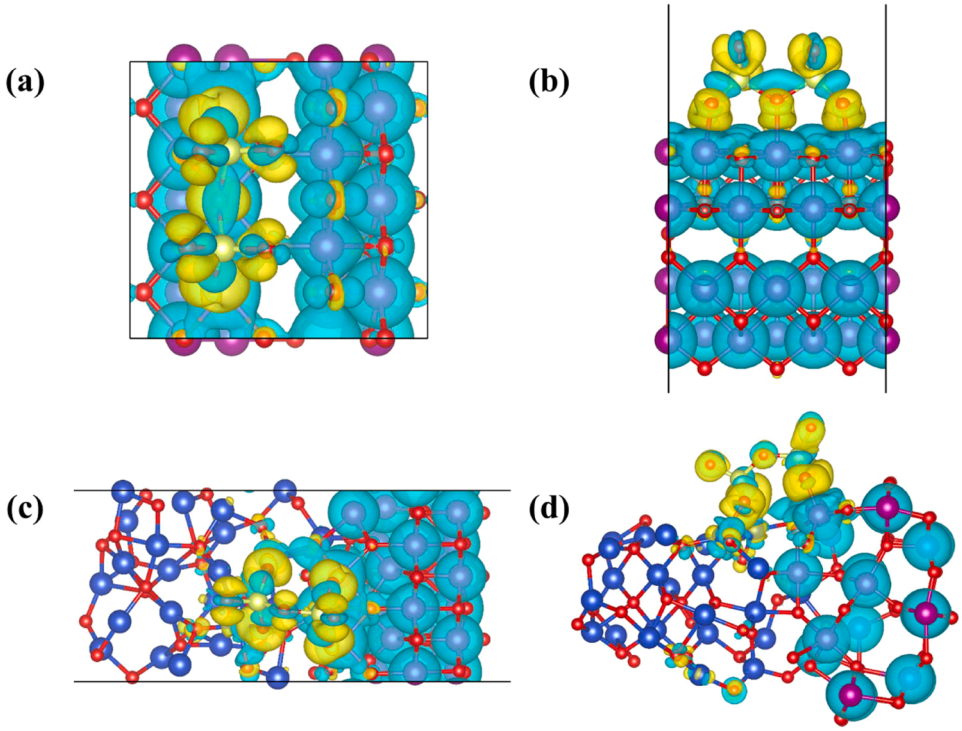

Fig. 6. Charge density difference of different catalysts. (a) Top and (b) side view of pyrophosphate-MnO_2 (200) and (c) top and (d) side view of pyrophosphate-CuO (002)/MnO_2 (200). The increase and decrease of charge accumulation are indicated by yellow and cyan area, respectively.

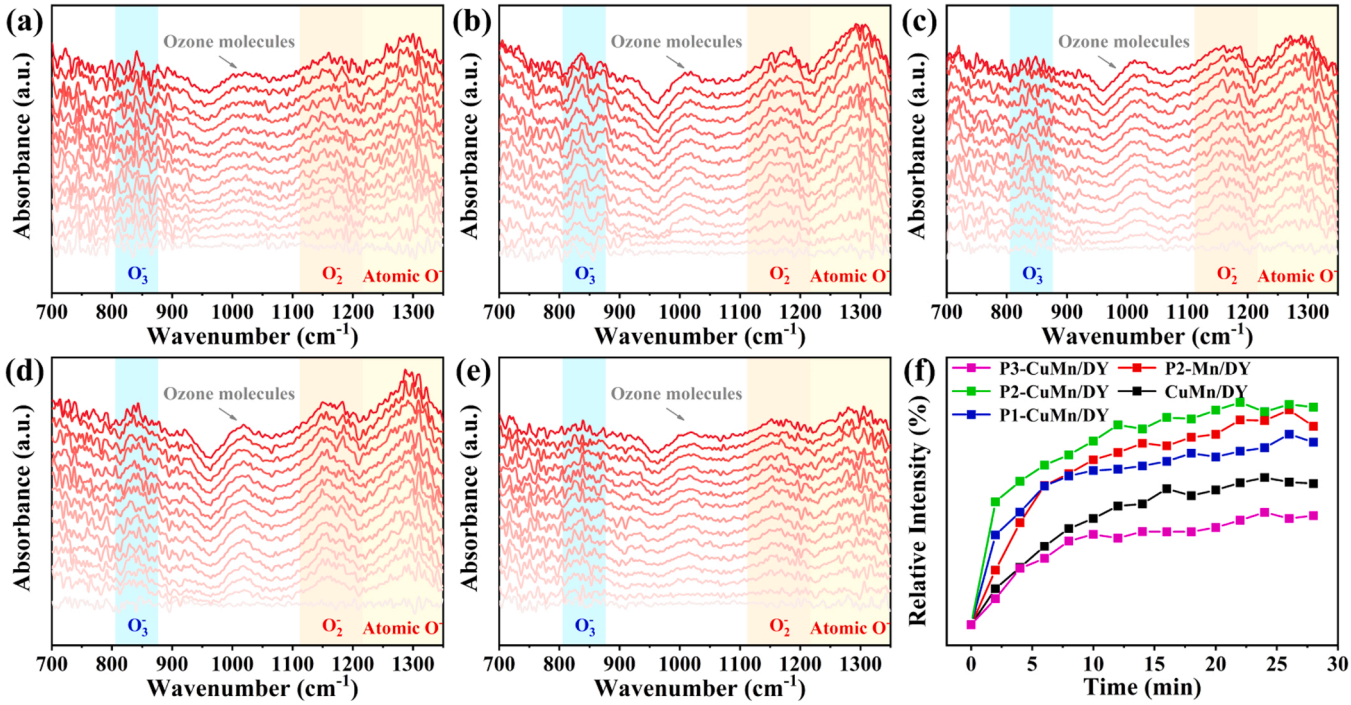

Fig. 7. *In situ* DRIFTS spectra of ozone adsorption over (a) CuMn/DY, (b) P2-Mn/DY, (c) P1-CuMn/DY, (d) P2-CuMn/DY and (e) P3-CuMn/DY, the spectra data recorded in every 2 min; (f) the relative intensity of atomic O^- accumulation on the surface of different catalysts within 30 min.

vacancies in the catalyst is sufficient.

3.4. Reaction mechanism

Fig. 8a-e shows *in situ* DRIFTS of catalytic oxidation reaction on different catalysts. Some similar reaction intermediates can be observed in all the catalysts, including alkoxide species (1028, 1060 and 1154 cm^{-1}) [46], benzaldehyde (1180 and 1679 cm^{-1}) [46], phenolic species (1280 cm^{-1}) [49], benzyl alcohol (1321 cm^{-1}) [50], maleic anhydride (1805 and 1930 cm^{-1}) [46]. Differently, benzoic acid (1417 cm^{-1}) [50], benzene (1479 cm^{-1}), phenol (1585 cm^{-1}) and quinone (1721 cm^{-1}) [51] can be detected in P2-Mn/DY, which cannot

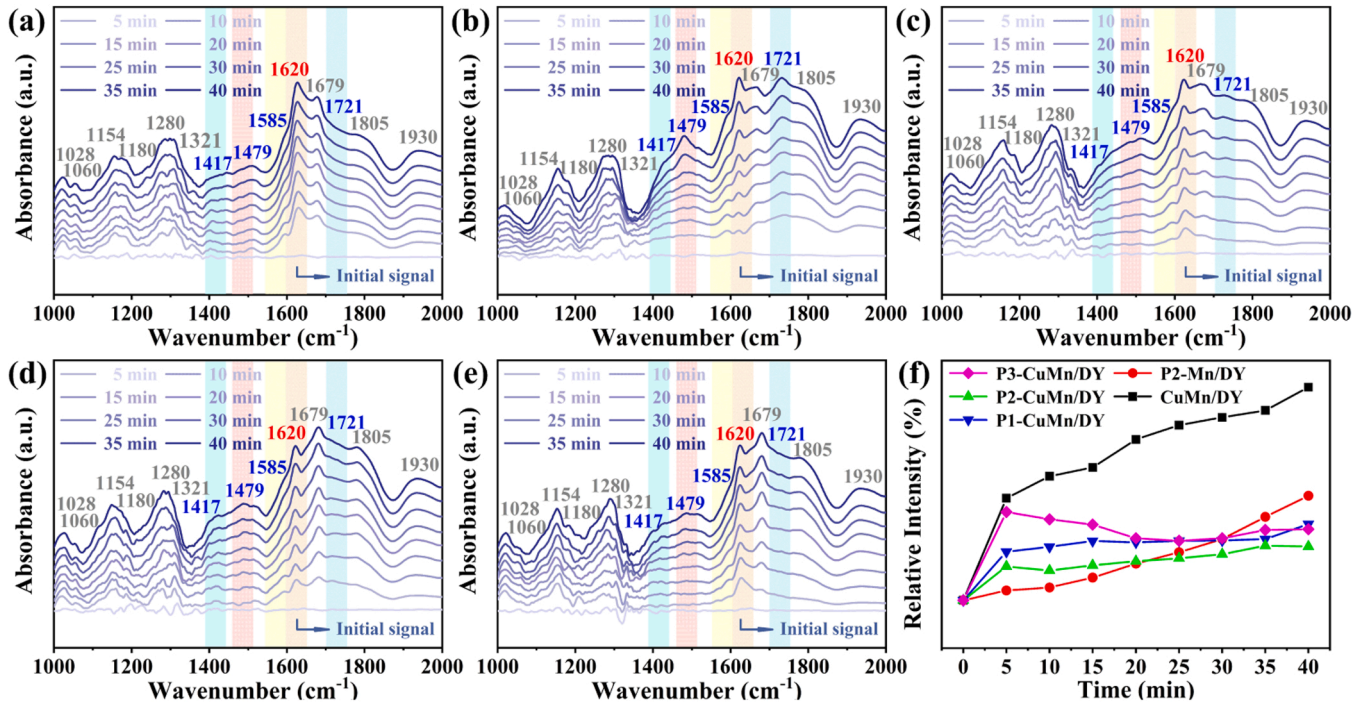

Fig. 8. *In situ* DRIFTS spectra of catalytic ozonation of toluene over (a) CuMn/DY, (b) P2-Mn/DY, (c) P1-CuMn/DY, (d) P2-CuMn/DY and (e) P3-CuMn/DY; (f) the relative intensity of bicarbonate accumulation on the surface of different catalysts within 40 min.

be observed in Cu-Mn catalysts. It is because that toluene can be directly ring-open when it is oxidized to benzoic acid due to the existent of CuOx (Fig. S17), reducing the accumulation of by-products and improving CO_2 selectivity of the catalysts (Fig. S6), which has been confirmed in the previous work [21]. Besides, another significant difference between the five catalysts comes from the peak signal detected at 1620 cm^{-1}, which can be attributed to bicarbonate [52]. Compared with CuMn/DY, the accumulation of bicarbonate in P-doped catalysts decreased significantly, which implied that the introduction of POx promoted the desorption of bicarbonate on the catalyst surface, accelerating the catalytic reaction rate. As shown in Fig. 8f, the accumulation of bicarbonate in P1-CuMn/DY, P2-CuMn/DY and P3-CuMn/DY not only decreased, but also tended to be dynamically stable after 20 min, which may suggest good catalytic performance of these catalysts. However, the catalytic activity of P3-CuMn/DY was poor, which can be attributed to the bad decomposition ability of ozone. Even though the bicarbonate accumulation of P2-Mn/DY was lower, it still showed an increasing trend with reaction time, which covered active sites and limited the toluene conversion of the catalysts. Therefore, the accumulation of bicarbonate on the catalyst surface may determine the catalytic ozonation rate of toluene.

4. Conclusions

In summary, the supported P-doped Cu-Mn catalysts were prepared by impregnation method. Different structures of phosphate (orthophosphate, pyrophosphate, polyphosphates) can be formed in the catalyst by controlling the phosphorus content. Appropriate P-doping improved the ozone utilization and promoted the conversion of toluene, it is because that the existence of pyrophosphate enhanced the interaction between Cu-Mn mixed oxides and the dealumination Y zeolite, resulting in an increase in the amount of Lewis acid sites and an enhancement in the activity of oxygen vacancy. However, excessive P-doping led to the increase of lattice oxygen ratio in the catalyst, which is not conducive to the decomposition of ozone, corresponding to the poor conversion of toluene. The characterization results of EPR, Raman and XPS etc. as well as DFT calculations showed that the newly formed Al-O-P bond in the zeolite support after P-doping can change the local loading environment of the metal nanoparticles, leading to an increase of electron cloud density and an enhancement of the oxygen vacancy activity around Cu-Mn mixed oxides, which is the key to influence the catalytic performance of the catalyst. In addition, the results of *in situ* DRIFTS showed that the accumulation of O* species on the surface of the catalyst has an important effect on the catalytic reaction. the activity of the oxygen vacancies determines the accumulation rate of O* when the amount of oxygen vacancies in the catalyst is sufficient. The desorption of bicarbonate on the catalyst surface is directly related to the degradation rate of toluene.

CRediT authorship contribution statement

Qi Shao: Investigation, Data curation, Methodology, Visualization, Writing – original draft. **Zihua Cheng:** Investigation, Data curation, Methodology. **Lei Gao:** Supervision, Validation. **Ting Li:** Supervision, Methodology. **Jian Zhang:** Funding acquisition, Data curation. **Chao Long:** Funding acquisition, Formal analysis, Project administration, Software, Validation, Writing – review & editing.

Declaration of Competing Interest

The authors declare that they have no known competing financial interests or personal relationships that could have appeared to influence the work reported in this paper.

Data availability

The authors are unable or have chosen not to specify which data has been used.

Acknowledgments

This research is financially supported by Natural Science Foundation of Jiangsu Province (BK20220786), Jiangsu Key Program of Science and Technology Demonstration for Social Development (BE2022838), and

Quanzhou City Science & Technology Program of China (2022NS008).

Appendix A. Supporting information

Supplementary data associated with this article can be found in the online version at doi:10.1016/j.apcatb.2023.123154.

References

[1] J. Zhang, Y. Zhao, C. Chen, Y.C. Huang, C.L. Dong, C.J. Chen, R.S. Liu, C. Wang, K. Yan, Y. Li, G. Wang, Tuning the coordination environment in single-atom catalysts to achieve highly efficient oxygen reduction reactions, J. Am. Chem. Soc. 141 (2019) 20118–20126.

[2] H. Wang, S. Sun, L. Nie, Z. Zhang, W. Li, Z. Hao, A review of whole-process control of industrial volatile organic compounds in China, J. Environ. Sci. (China) 123 (2023) 127–139.

[3] K. Zhang, H. Ding, W. Pan, X. Mu, K. Qiu, J. Ma, Y. Zhao, J. Song, Z. Zhang, Research progress of a composite metal oxide catalyst for VOC degradation, Environ. Sci. Technol. 56 (2022) 9220–9236.

[4] B. Liu, J. Ji, B. Zhang, W. Huang, Y. Gan, D.Y.C. Leung, H. Huang, Catalytic ozonation of VOCs at low temperature: A comprehensive review, J. Hazard. Mater. 422 (2022), 126847.

[5] D. Ma, W. Liu, Y. Huang, D. Xia, Q. Lian, C. He, Enhanced catalytic ozonation for eliminating CH_3SH via stable and circular electronic metal-support interactions of Si-O-Mn bonds with low Mn loading, Environ. Sci. Technol. 56 (2022) 3678–3688.

[6] R. Yang, P. Han, Y. Fan, Z. Guo, Q. Zhao, Y. Wang, S. Che, S. Lin, R. Zhu, The performance and reaction pathway of delta-MnO_2/USY for catalytic oxidation of toluene in the presence of ozone at room temperature, Chemosphere 247 (2020), 125864.

[7] G. Chen, Z. Wang, F. Lin, Z. Zhang, H. Yu, B. Yan, Z. Wang, Comparative investigation on catalytic ozonation of VOCs in different types over supported MnOx catalysts, J. Hazard. Mater. 391 (2020), 122218.

[8] Z.B. Sun, Y.N. Si, S.N. Zhao, Q.Y. Wang, S.Q. Zang, Ozone decomposition by a manganese-organic framework over the entire humidity range, J. Am. Chem. Soc. 143 (2021) 5150–5157.

[9] S. Zhao, Y. Yang, F. Bi, Y. Chen, M. Wu, X. Zhang, G. Wang, Oxygen vacancies in the catalyst: Efficient degradation of gaseous pollutants, Chem. Eng. J. 454 (2023), 140376.

[10] Y. Zheng, K. Fu, Z. Yu, Y. Su, R. Han, Q. Liu, Oxygen vacancies in a catalyst for VOCs oxidation: Synthesis, characterization, and catalytic effects, J. Mater. Chem. A 10 (2022) 14171–14186.

[11] K. Yu, L.L. Lou, S. Liu, W. Zhou, Asymmetric oxygen vacancies: the intrinsic redox active sites in metal oxide catalysts, Adv. Sci. 7 (2020) 1901970.

[12] J. Zhang, K. Wu, J. Xiong, Q. Ren, J. Zhong, H. Cai, H. Huang, P. Chen, J. Wu, L. Chen, M. Fu, D. Ye, Static and dynamic quantification tracking of asymmetric oxygen vacancies in copper-ceria catalysts with superior catalytic activity, Appl. Catal. B: Environ. 316 (2022), 121620.

[13] Y. Deng, Z. Zhou, H. Zeng, R. Tang, L. Li, J. Wang, C. Feng, D. Gong, L. Tang, Y. Huang, Phosphorus and kalium co-doped g-C_3N_4 with multiple-locus synergies to degrade atrazine: Insights into the depth analysis of the generation and role of singlet oxygen, Appl. Catal. B: Environ. 320 (2023), 121942.

[14] X. Chen, Y. Zheng, Y. Chen, Y. Xu, F. Zhong, W. Zhang, Y. Xiao, Y. Zheng, Improved methane oxidation activity of P-doped γ-Al_2O_3 supported palladium catalysts by tailoring the oxygen mobility and electronic properties, Int. J. Hydrog. Energy 44 (2019) 27772–27783.

[15] X. Yu, L. Dai, Y. Peng, J. Deng, Y. Liu, L. Jing, X. Zhang, Z. Hou, J. Wang, H. Dai, High selectivity to HCl for the catalytic removal of 1,2-dichloroethane over RuP/3DOM WOx: Insights into the effects of P-doping and H_2O introduction, Environ. Sci. Technol. 55 (2021) 14906–14916.

[16] Z. Huang, S. Cao, J. Yu, X. Tang, Y. Guo, Y. Guo, L. Wang, S. Dai, W. Zhan, Total oxidation of light alkane over phosphate-modified Pt/CeO_2 catalysts, Environ. Sci. Technol. 56 (2022) 9661–9671.

[17] H. Ma, X. Wang, T. Tan, X. Zhou, F. Dong, Y. Sun, Stabilize the oxygen vacancies in Bi_2SiO_5 for durable photocatalysis via altering local electronic structure with phosphate dopant, Appl. Catal. B: Environ. 319 (2022), 121911.

[18] S. Zhou, H. Jang, Q. Qin, L. Hou, M.G. Kim, S. Liu, X. Liu, J. Cho, Boosting hydrogen evolution reaction by phase engineering and phosphorus doping on Ru/P-TiO_2, Angew. Chem. Int. Ed. Engl. 61 (2022), e202212196.

[19] H. Guo, Q. Feng, K. Xu, J. Xu, J. Zhu, C. Zhang, T. Liu, Self-templated conversion of metallogel into heterostructured TMP@carbon quasiaerogels boosting bifunctional electrocatalysis, Adv. Funct. Mater. 29 (2019) 1903660.

[20] H.E. van der Bij, B.M. Weckhuysen, Phosphorus promotion and poisoning in zeolite-based materials: Synthesis, characterisation and catalysis, Chem. Soc. Rev. 44 (2015) 7406–7428.

[21] Q. Shao, S. Wei, X. Hu, H. Dong, T. Wen, L. Gao, C. Long, Tuning the micro-coordination environment of Al in dealumination Y zeolite to enhance electron transfer at the Cu-Mn oxides interface for highly efficient catalytic ozonation of toluene at low temperatures, Environ. Sci. Technol. 56 (2022) 15449–15459.

[22] Q. Shao, H. Dong, J. Zhang, B. Xu, Y. Wu, C. Long, Manganese supported on controlled dealumination Y-zeolite for ozone catalytic oxidation of low concentration toluene at low temperature, Chemosphere 271 (2021), 129604.

[23] N. Xue, L. Nie, D. Fang, X. Guo, J. Shen, W. Ding, Y. Chen, Synergistic effects of tungsten and phosphorus on catalytic cracking of butene to propene over HZSM-5, Appl. Catal. A: Gen. 352 (2009) 87–94.

[24] K. Chen, X. Wu, J. Zhao, H. Zhao, A. Li, Q. Zhang, T. Xia, P. Liu, B. Meng, W. Song, X. Zhu, H. Liu, X. Gao, C. Xu, B. Shen, Organic-free modulation of the framework Al distribution in ZSM-5 zeolite by magnesium participated synthesis and its impact on the catalytic cracking reaction of alkanes, J. Catal. 413 (2022) 735–750.

[25] A. Bazyari, A.A. Khodadadi, N. Hosseinpour, Y. Mortazavi, Effects of steaming-made changes in physicochemical properties of Y-zeolite on cracking of bulky 1,3,5-triisopropylbenzene and coke formation, Fuel Process. Technol. 90 (2009) 1226–1233.

[26] A.B. Pinar, P. Rzepka, A.J. Knorpp, L.B. McCusker, C. Baerlocher, T. Huthwelker, J. A. van Bokhoven, Pinpointing and quantifying the aluminum distribution in zeolite catalysts using anomalous scattering at the Al absorption edge, J. Am. Chem. Soc. 143 (2021) 17926–17930.

[27] X. Chen, X. Zheng, W. Lin, D. Chen, Y. Zheng, L. Jiang, Adsorption property and catalytic performance over ordered mesoporous phosphorus-doped Pd-alumina catalysts, Powder Technol. 338 (2018) 869–877.

[28] N.C. Nelson, Z. Wang, P. Naik, J.S. Manzano, M. Pruski, I.I. Slowing, Phosphate modified ceria as a Brønsted acidic/redox multifunctional catalyst, J. Mater. Chem. A 5 (2017) 4455–4466.

[29] R. Huang, B. Wan, M. Hultz, J.M. Diaz, Y. Tang, Phosphatase-mediated hydrolysis of linear polyphosphates, Environ. Sci. Technol. 52 (2018) 1183–1190.

[30] Q. Shao, M. Yang, A. Li, S. Wei, X. Hu, C. Long, Enhanced catalytic ozonation of toluene using supported MnOx/USY via regulating the distribution of aluminum species in USY by dealumination, J. Environ. Chem. Eng. 10 (2022), 108604.

[31] J. Shao, F. Lin, Z. Wang, P. Liu, H. Tang, Y. He, K. Cen, Low temperature catalytic ozonation of toluene in flue gas over Mn-based catalysts: Effect of support property and SO_2/water vapor addition, Appl. Catal. B: Environ. 266 (2020), 118662.

[32] Y. Zhu, B. Li, C. Zhao, Cu nanoparticles supported on core–shell MgO-La_2O_3 catalyzed hydrogenolysis of furfuryl alcohol to pentanediol, J. Catal. 410 (2022) 42–53.

[33] H.C. Wang, H.P. Wang, K.S. Lin, Adsorption of pyridine on dealuminated zeolite HY, J. Environ. Sci. Health, Part A 34 (1999) 1849–1858.

[34] W. Wang, W. Zhang, Y. Chen, X. Wen, H. Li, D. Yuan, Q. Guo, S. Ren, X. Pang, B. Shen, Mild-acid-assisted thermal or hydrothermal dealumination of zeolite beta, its regulation to Al distribution and catalytic cracking performance to hydrocarbons, J. Catal. 362 (2018) 94–105.

[35] G. Busca, Acidity and basicity of zeolites: A fundamental approach, Microporous Mesoporous Mater. 254 (2017) 3–16.

[36] X. Zhang, X. Liu, Y. Zeng, Y. Tong, X. Lu, Oxygen defects in promoting the electrochemical performance of metal oxides for supercapacitors: recent advances and challenges, Small Methods 4 (2020) 1900823.

[37] J. Wu, J. Gao, S. Lian, J. Li, K. Sun, S. Zhao, Y.D. Kim, Y. Ren, M. Zhang, Q. Liu, Z. Liu, Z. Peng, Engineering the oxygen vacancies enables Ni single-atom catalyst for stable and efficient C-H activation, Appl. Catal. B: Environ. 314 (2022), 121516.

[38] I. Halasz, M. Agarwal, B. Marcus, W.E. Cormier, Molecular spectra and polarity sieving of aluminum deficient hydrophobic H-Y zeolites, Microporous Mesoporous Mater. 84 (2005) 318–331.

[39] Y. Meng, H.C. Genuino, C.H. Kuo, H. Huang, S.Y. Chen, L. Zhang, A. Rossi, S. L. Suib, One-step hydrothermal synthesis of manganese-containing MFI-type zeolite, Mn-ZSM-5, characterization, and catalytic oxidation of hydrocarbons, J. Am. Chem. Soc. 135 (2013) 8594–8605.

[40] L. Debbichi, M.C. Marco de Lucas, J.F. Pierson, P. Krüger, Vibrational properties of CuO and Cu_4O_3 from first-principles calculations, and Raman and infrared spectroscopy, J. Phys. Chem. C. 116 (2012) 10232–10237.

[41] G. Zhu, J. Zhu, W. Jiang, Z. Zhang, J. Wang, Y. Zhu, Q. Zhang, Surface oxygen vacancy induced α-MnO_2 nanofiber for highly efficient ozone elimination, Appl. Catal. B: Environ. 209 (2017) 729–737.

[42] Q. Tang, X. Gong, P. Zhao, Y. Chen, Y. Yang, Copper–manganese oxide catalysts supported on alumina: Physicochemical features and catalytic performances in the aerobic oxidation of benzyl alcohol, Appl. Catal. A: Gen. 389 (2010) 101–107.

[43] L. Jia, J. Liu, D. Huang, J. Zhao, J. Zhang, K. Li, Z. Li, W. Zhu, Z. Zhao, J. Liu, Interface engineering of a bifunctional Cu-SSZ-13@CZO core–shell catalyst for boosting potassium ion and SO_2 tolerance, ACS Catal. 12 (2022) 11281–11293.

[44] F. Wang, J. Deng, S. Impeng, Y. Shen, T. Yan, G. Chen, L. Shi, D. Zhang, Unraveling the effects of the coordination number of Mn over α-MnO_2 catalysts for toluene oxidation, Chem. Eng. J. 396 (2020), 125192.

[45] C. He, Y. Wang, Z. Li, Y. Huang, Y. Liao, D. Xia, S. Lee, Facet Engineered alpha-MnO_2 for efficient catalytic ozonation of odor CH_3SH: Oxygen vacancy-induced active centers and catalytic mechanism, Environ. Sci. Technol. 54 (2020) 12771–12783.

[46] S. Mo, Q. Zhang, J. Li, Y. Sun, Q. Ren, S. Zou, Q. Zhang, J. Lu, M. Fu, D. Mo, J. Wu, H. Huang, D. Ye, Highly efficient mesoporous MnO_2 catalysts for the total toluene oxidation: Oxygen-vacancy defect engineering and involved intermediates using in situ DRIFTS, Appl. Catal. B: Environ. 264 (2020), 118464.

[47] H. Valdés, F.J. Ulloa, V.A. Solar, M.S. Cepeda, F. Azzolina-Jury, F. Thibault-Starzyk, New insight of the influence of acidic surface sites of zeolite on the ability to remove gaseous ozone using operando DRIFTS studies, Microporous Mesoporous Mater. 294 (2020), 109912.

[48] J. Wu, T. Su, Y. Jiang, X. Xie, Z. Qin, H. Ji, *In situ* DRIFTS study of O_3 adsorption on CaO, γ-Al_2O_3, CuO, α-Fe_2O_3 and ZnO at room temperature for the catalytic ozonation of cinnamaldehyde, Appl. Surf. Sci. 412 (2017) 290–305.

[49] H. Zhang, S. Sui, X. Zheng, R. Cao, P. Zhang, One-pot synthesis of atomically dispersed Pt on MnO_2 for efficient catalytic decomposition of toluene at low temperatures, Appl. Catal. B: Environ. 257 (2019), 117878.
[50] J. Li, H. Na, X. Zeng, T. Zhu, Z. Liu, *In situ* DRIFTS investigation for the oxidation of toluene by ozone over Mn/HZSM-5, Ag/HZSM-5 and Mn–Ag/HZSM-5 catalysts, Appl. Surf. Sci. 311 (2014) 690–696.
[51] J. Zhong, Y. Zeng, D. Chen, S. Mo, M. Zhang, M. Fu, J. Wu, Z. Su, P. Chen, D. Ye, Toluene oxidation over Co^{3+}-rich spinel Co_3O_4: Evaluation of chemical and by-product species identified by in situ DRIFTS combined with PTR-TOF-MS, J. Hazard. Mater. 386 (2020), 121957.
[52] D.Z. Zhao, C. Shi, X.S. Li, A.M. Zhu, B.W. Jang, Enhanced effect of water vapor on complete oxidation of formaldehyde in air with ozone over MnOx catalysts at room temperature, J. Hazard. Mater. 239–240 (2012) 362–369.